View metadata, citation and similar papers at core.ac.uk

brought to you by CORE

provided by UNL | Libraries

University of Nebraska - Lincoln

DigitalCommons@University of Nebraska - Lincoln

Faculty Publications, Department of Physics and Astronomy

Research Papers in Physics and Astronomy

2010

The electronic structure of Li2B4O7(110) and Li2B4O7(100)

D. W. Wooten

I. Ketsman

J. Xiao

Ya. B. Losovyj

J. Petrosky

See next page for additional authors

Follow this and additional works at: https://digitalcommons.unl.edu/physicsfacpub

This Article is brought to you for free and open access by the Research Papers in Physics and Astronomy at DigitalCommons@University of Nebraska - Lincoln. It has been accepted for inclusion in Faculty Publications, Department of Physics and Astronomy by an authorized administrator of DigitalCommons@University of Nebraska - Lincoln.

Authors

D. W. Wooten, I. Ketsman, J. Xiao, Ya. B. Losovyj, J. Petrosky, J. McClory, Ya. V. Burak, V. T. Adamiv, J. M. Brown, and P. A. Dowben

Eur. Phys. J. Appl. Phys. **52**, 31601 (2010)
DOI: 10.1051/epjap/2010160

THE EUROPEAN PHYSICAL JOURNAL APPLIED PHYSICS

Regular Article

The electronic structure of $Li_2B_4O_7(110)$ and $Li_2B_4O_7(100)$

D. Wooten[1], I. Ketsman[2], J. Xiao[2], Ya.B. Losovyj[2,3], J. Petrosky[1], J. McClory[1], Ya.V. Burak[4], V.T. Adamiv[4], J.M. Brown[5], and P.A. Dowben[2,a]

[1] Air Force Institute of Technology, 2950 Hobson Way, Wright-Patterson Air Force Base, OH 45433-7765, USA
[2] Department of Physics and Astronomy and the Nebraska Center for Materials and Nanoscience, University of Nebraska-Lincoln, P.O. Box 880111, Lincoln, NE 68588-0111, USA
[3] J. Bennett Johnston Sr. Center for Advanced Microstructures and Devices, Louisiana State University, 6980 Jefferson Highway, Baton Rouge, LA 70806, USA
[4] Institute of Physical Optics, Dragomanov 23, Lviv 79005, Ukraine
[5] Cincinatti Children's Hospital Medical Center, 32344 Burnet Avenue, Cincinatti, OH, USA

Received: 31 May 2010 / Accepted: 13 August 2010
Published online: 30 November 2010 – © EDP Sciences

Abstract. The band structure of $Li_2B_4O_7(100)$ and $Li_2B_4O_7(110)$ was experimentally determined using a combination of angle-resolved photoemission and angle-resolved inverse photoemission spectroscopies. The experimental band gap depends on crystallographic direction but exceeds 8.8 eV, while the bulk band gap is believed to be in the vicinity of 9.8 eV, in qualitative agreement with expectations. The occupied bulk band structure indicates relatively large values for the hole mass; with the hole mass as significantly larger than that of the electron mass derived from the unoccupied band structure. The $Li_2B_4O_7(110)$ surface is characterized by a very light mass image potential state and a surface state that falls within the band gap of the projected bulk band structure.

1 Introduction

Lithium tetraborate is pyroelectric material, of space group of $I4_1cd$, and a rather complex tetragonal crystal with 104 atoms per unit cell [1–6] with an appreciable pyroelectric coefficient in the region of 100 K to 250 K [7–9]. While several band structure calculations exist [10,11], there is no uniform consistency in the predicted band structure. Recent density functional theory (DFT) band structure calculations [10] suggest that the hole mass is larger than the electron mass, that is to say that the dispersion of the valence bands is expected to be very small compared to the band dispersion in the conduction bands. There has been, however, no experimental confirmation of any of the key predictions of the calculated band structure, except the band gap [9,11–13] and some of the optical properties [11].

The lithium borates have been considered as possible solid state neutron detectors [14,15], an application where efficient charge collection is desirable. The pyroelectric and piezoelectric properties of the lithium borates require excellent dielectric properties in the crystals of $Li_2B_4O_7$, particularly along the polar [001] direction. This material has been measured to have undoped resistivities on the order of 10^{10} Ω cm [14] or more. This problem of very high resistivities has been circumvented in semiconducting boron carbides where filling impurity bands [16,17] appear to lead to dramatic increases in carrier mobilities in materials with otherwise very large carrier effective masses [17]. Thus semiconducting boron carbides do make effective solid state neutron detectors [18–25]. Similar alloying of lithium tetraborate may also result in an effective semiconductor. Although undoped lithium tetraborate has an estimated large 6.2 to 9.3 eV band gap [9–12], the material does possess advantages for solid state neutron detection if suitably band engineered semiconductor device grade materials can be fabricated. $Li_2B_4O_7$ has been enriched to 95 at% ^{6}Li and 97.3 at% ^{10}B from the natural 7.4 at% ^{6}Li and 19 at% ^{10}B [15]. It has been shown that this material can be doped [9,26,27], so impurity level band "engineering" of lithium tetraborate ($Li_2B_4O_7$) should be possible.

2 Experimental

The $Li_2B_4O_7$ single crystals were grown from the melt by the Czochralski technique as described elsewhere [9,15] and (110) and (100) crystals were cut with a miscut of no more than 0.5°, as determined by X-ray diffraction. As noted at the outset, lithium tetraborate is a tetragonal crystal [1–6], consisting of boron-oxygen complexes of planar trigonal BO_3 and tetrahedral BO_4 groups.

[a] *Corresponding author:* Department of Physics and Astronomy, Theodore Jorgensen Hall, University of Nebraska-Lincoln, 855 North 16th Street, Lincoln, NE 68588-0299, USA
e-mail: pdowben@unl.edu

Article published by EDP Sciences

This document is a U.S. government work and is not subject to copyright in the United States.

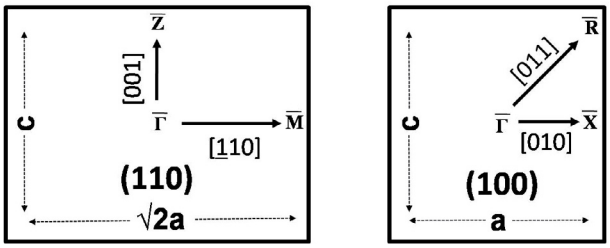

Fig. 1. Schematic of both the $Li_2B_4O_7(100)$ and $Li_2B_4O_7(110)$ surfaces investigated here, depicting the four directions used in the band mapping studies and denoting the real space lattice but with the labels for the Brillouin zone critical points included. The lattice parameters that characterize the surface unit cells have been determined to be $a = 9.477$ Å and $c = 10.286$ Å [1–6], as schematically illustrated.

Lattice parameters that characterize the unit cell have been determined to be $a = 9.477$ Å and $c = 10.286$ Å [5], as schematically illustrated in Figure 1 for both the $Li_2B_4O_7(100)$ and $Li_2B_4O_7(110)$ surfaces investigated here.

While the X-ray diffraction shows that the crystals were well oriented and single phase, point defects comprising of isolated oxygen vacancies, and to a smaller extent isolated lithium vacancies, with a very small trace of Cu impurities were evident in electron paramagnetic resonance (EPR) and electron-nuclear double resonance (ENDOR), consistent with prior measurements [5,28]. These isolated point defects, amounting to between 2 and 5 ppm in total, were not sufficient to degrade our crystals. Clean surfaces were prepared by several methods including resistive heating and combinations of sputtering and subsequent annealing. The electronic structure and stoichiometry were similar in all cases.

Both the occupied and unoccupied experimental band structures were characterized by combined angle-resolved ultraviolet photoemission spectroscopy (ARUPS) and angle-resolved inverse photoemission spectroscopy (ARIPES) studies of the $Li_2B_4O_7(100)$ and $Li_2B_4O_7(110)$ single crystal surfaces. The angle-resolved photoemission experiments were performed using the 3 m toroidal grating monochromator (3 m TGM) beam line [29,30] at the Center for Advanced Microstructures and Devices [31] in an ultra high vacuum (UHV) chamber previously described [29,30], equipped with a hemispherical electron analyzer with an angular acceptance of ±1°, as described elsewhere. The combined resolution of the electron energy analyzer and monochromator was 120–150 meV for photon energies in the range of 50–120 eV. The photoemission experiments were undertaken with a light incidence angle of 45° with respect to the surface normal, unless stated otherwise. The photoelectrons were collected at emission angles stated in terms of the surface normal. For the light polarization dependent photoemission experiments the light incidence angles were varied, in order to change the orientation of the **E** of the plane-polarized incident light, but the photo-electrons were collected along the surface normal ($\overline{\Gamma}$) to preserve the high point group symmetry. The angle-resolved photoemission measurements were made at sample temperatures over a temperature range from 250 K to 700 K [9,13,29,30,32].

The angle-resolved (wave vector or k-resolved) inverse photoemission spectra were also taken to determine the unoccupied band structure [33–35]. The angle-resolved inverse photoemission spectra were obtained by using variable energy electrons incident at different angles with respect to the sample surface normal, while measuring the emitted photons at a fixed energy (9.7 eV) using a Geiger-Müller detector with an instrumental linewidth of about 400 meV [36,37]. The inverse photoemission spectra were taken with sample temperatures of 300 to 350 K, as there was much less surface charging evident in inverse photoemission compared with the photoemission experiments.

The preponderance of the angle-resolved photoemission data was gathered at 623 ± 5 K. There was considerable photovoltaic charging below 620 K in the photoemission spectra [9,13], as expected because the lithium tetraborate crystals are dielectrics. At temperatures above 620 K, the surface photovoltaic charging effects were negligible [13] and the charges within the crystal, including the trapped charges, exhibit increased mobility [9].

The reference of the observed binding energies to the Fermi level for $Li_2B_4O_7(110)$, and $Li_2B_4O_7(100)$, as done here, differs from the sometimes common practice of assigning binding energies with respect to the valence band maximum for lithium borate [10]. Prior studies of lithium tetraborate also have assigned their binding energies with respect to the chemical potential or Fermi level [9,12,13,38]. We chose this latter convention for these investigations, i.e. choosing the Fermi level as a reference, and citing binding energies in terms of E-E_F. Checks to the placement of the Fermi level in both the angle-resolved photoemission and inverse photoemission experiments were performed using tantalum films in electrical contact with the samples [9,12,32]. Surface charging effects in the photoemission experiments were also taken into account by using the Li1s and O2s shallow core levels as a reference [12,13].

3 The valence to conduction band gaps of $Li_2B_4O_7(110)$ and $Li_2B_4O_7(100)$

Both $Li_2B_4O_7(100)$ and $Li_2B_4O_7(110)$ exhibit a density of states that qualitatively agrees with the results from model bulk band structure calculations for $Li_2B_4O_7$ [10,11], as seen in Figure 2. For $Li_2B_4O_7(100)$ the band gaps obtained from combined photoemission and inverse photoemission are 10.1 ± 0.5 eV and 8.9 ± 0.5 eV with the in-plane component of **E** aligned along the [011] and [010] direction, respectively. For $Li_2B_4O_7(110)$, the band gaps are 9.8 ± 0.5 eV in both the [001] and [$\underline{1}$10] direction. In general, the combined photoemission and inverse photoemission measure the direct band gap, but as final state spectroscopies. Consequently, perfect agreement with a ground state calculation, such as density functional theory, is generally not possible and unlikely; although the

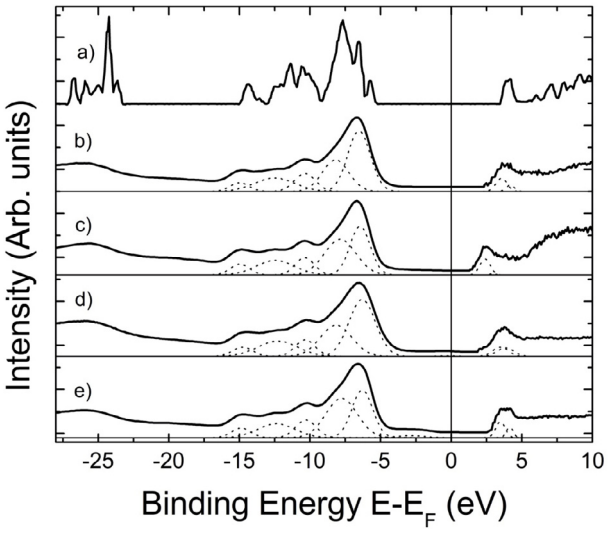

Fig. 2. A comparison of the combined experimental photoemission (left) and inverse photoemission (right) data, in E-E_F, with theoretical expectations. The theoretical density of the bulk band states of crystalline $Li_2B_4O_7$ (a) obtained by the LDA PW1PW is adapted from Islam et al. [10]. The combined experimental photoemission (left) and inverse photoemission (right) data for $Li_2B_4O_7$(100), with the in-plane component of the incident light **E** for photoemission oriented along (b) [011] and (c) [010] are shown along with the data for $Li_2B_4O_7$(110) with the in-plane component of the incident light **E** for photoemission oriented along (d) [001] and (e) [$\underline{1}$10]. For the photoemission, the photon energy is 56 eV and the synchrotron light is incident at 45 degrees with respect to the surface normal. The electrons were either collected along the surface normal (photoemission) or incident along the surface normal (inverse photoemission).

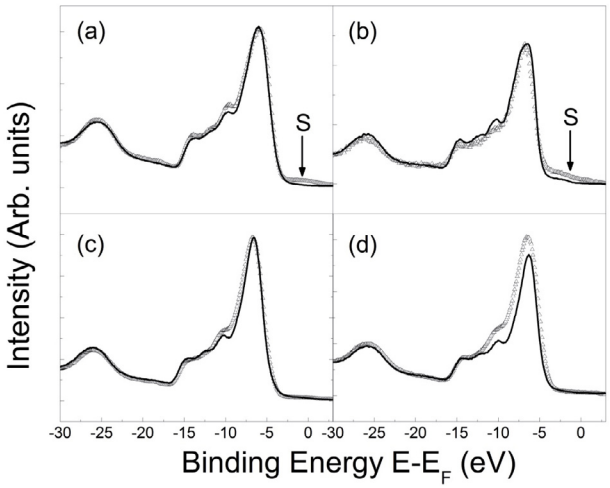

Fig. 3. The light polarization dependent photoemission spectra for the (a), (b) $Li_2B_4O_7$(110) and (c), (d) $Li_2B_4O_7$(100) surfaces. The in-plane component of the incident light **E** for photoemission from $Li_2B_4O_7$(110) oriented along (a) [001] or (b)[$\underline{1}$10]. For $Li_2B_4O_7$(100), the incident light **E** for photoemission was oriented along [011] (c) or [010] (d). The orientation of light incidence angle was either 70 degrees {-Δ – Δ – Δ-} or 45 degrees {——} with respect to surface normal and the spectra were taken with a photon energy of 70 eV with the photoelectrons collected along the surface normal. The (S) denotes a surface state. The occupied state binding energies are given in terms of E-E_F.

agreement as seen here between experiment and the prior band structure calculations [10] is generally quite good.

The Fermi level is placed slightly closer to the conduction band edge in the combined experimental photoemission and inverse photoemission spectra, as seen in Figure 2. This indicates that both the $Li_2B_4O_7$(100) and $Li_2B_4O_7$(110) surfaces are n-type, although (100) is more n-type than (110). While we have not measured the majority carrier, the Fermi level placement is consistent with the known bulk properties where the majority of defects seen in these $Li_2B_4O_7$(100) and $Li_2B_4O_7$(110) were oxygen vacancies.

It is evident in the combined experimental photoemission and inverse photoemission studies (Fig. 2) that there are differences between the band gap values, in particular for $Li_2B_4O_7$(100) with in-plane component of **E** preferentially aligned along the [010] versus [011] directions. Inverse photoemission tends to be much more surface sensitive than photoemission. The observed placement of the conduction band edge closer to the Fermi level with the photon collection direction along one specific crystallographic direction does suggest surface states of preferential symmetry or selected oxygen vacancies at the $Li_2B_4O_7$(100) surface. There exists data to support both of these contentions.

4 Surface states within the gap of the projected bulk band structure

In general, there is little light polarization dependence observed in the photoemission spectra taken for both the $Li_2B_4O_7$(100) and $Li_2B_4O_7$(110) surfaces. As seen in Figures 3a and 3b, the light polarization dependent photoemission in the valence band region of the $Li_2B_4O_7$(110) surface exhibits few differences between a light incidence angle of 70°, placing the electric vector **E** more along the surface normal and a light incidence angle of 45°. Yet with a light incidence angle of 70°, there is a small density of states within the gap placed close to the Fermi level, as seen in Figures 3a and 3b. This region, with the presence of surface states located within the bulk band gap and below E_F, has been marked by an "S" in Figure 3, and has been enhanced in Figure 4.

As these $Li_2B_4O_7$(110) surface states fall into the gap of the projected bulk band structure (Fig. 2a) [10], we can initially conclude that these observed occupied states are in fact true surface states. The observed intensities of these surface states in photoemission are clearly affected by light polarization (Figs. 3a and 3b) and these surface states are likely of s or p_z character (with z along the surface normal), given that they are enhanced with incident light where the electric vector **E** is more along the

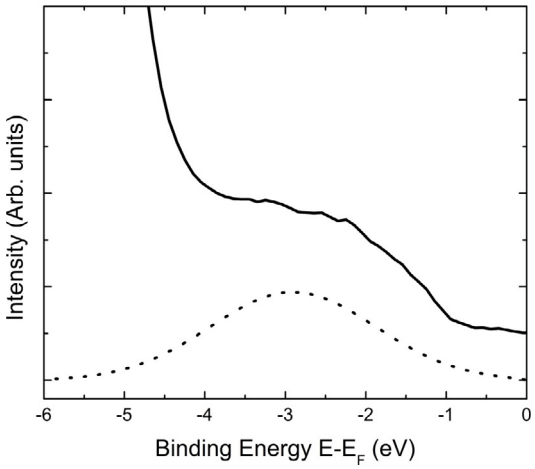

Fig. 4. Angle resolved photoemission spectrum (ARPES) (—) for the $Li_2B_4O_7(110)$ surface illustrating the presence of an occupied surface state within the gap of the projected bulk band structure (- - -) that does not include contributions from the valence band maximum or background. The spectrum was taken at a photon energy of 56 eV, with a light incidence angle of 70 degrees with respect to sample surface normal and the in-plane component of the incident light **E** oriented along the [001] direction. The occupied state binding energies are given in terms of E-E_F.

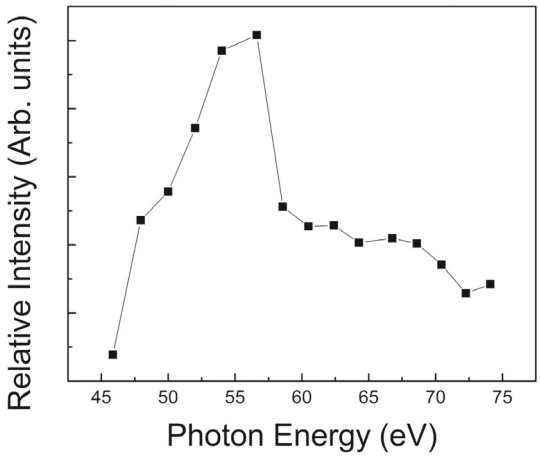

Fig. 5. The relative peak intensity near the valence band maximum (-6.7 ± 0.2 eV, E-E_F) versus photon energy depicting resonance for the $Li_2B_4O_7(110)$ surface. For all spectra, the in-plane component of the incident light **E** is oriented along [001], the light incidence angle was 45 degrees, and the photoelectrons were collected along the surface normal. Data was abstracted from a sequence of photoemission spectra such as those shown in Figure 6.

surface normal. Certainly for the $Li_2B_4O_7(110)$ surface, the possibility of surface states must be given serious consideration as a Li1s surface to bulk core level shift has been observed for this surface [12]. The presence of surface states for semiconductors and insulators is certainly not new [39,40], but these are the first examples reported for $Li_2B_4O_7$ (110). For the $Li_2B_4O_7(100)$ surface, the absence of such states within the gap between the valence band edge and the Fermi level (Figs. 2b, 2c, 3c and 3d), in the vicinity of the Fermi level, along with a decrease in the conduction band minimum, with the photons collected along [010] (Fig. 2c), is consistent with some types of defects at this surface.

For the $Li_2B_4O_7(100)$, there is enhancement of the valence band photoemission intensities where the incident photon electric vector **E** is more along the surface normal and in-plane component of the incident light **E** is oriented along the [010] direction (Fig. 3d). It is this surface and crystallographic orientation where the conduction band edge is placed closest to the Fermi level in inverse photoemission (Fig. 2c), as just noted. Both the light polarization dependence and the conduction band edge placement for this orientation of the $Li_2B_4O_7(100)$ surface could be explained by an increased number of oxygen vacancies. The loss of surface oxygen coordinated by O2p_x orbitals, with x in-plane and using the surface lattice notation of Figure 1, would lead to a more polar $Li_2B_4O_7(100)$ surface.

Both the $Li_2B_4O_7(100)$ and $Li_2B_4O_7(110)$ surfaces are orthogonal to the polar and pyroelectric [001] direction of $Li_2B_4O_7$ [7–9], and are not, a priori, hugely polar surfaces which generally are unstable against surface reconstructions. This makes surface defects an even more likely cause of the light polarization dependent photoemission observed for the $Li_2B_4O_7(100)$ surface, with the in-plane component of the incident photon **E** aligned along [010] or perpendicular to the polar direction [001]. The resulting photoemission from the $Li_2B_4O_7(100)$ loses any even symmetry mirror plane in the photoemission symmetry selection rules [33,41–43]. It is also telling that the image states [44], discussed below, seen for the $Li_2B_4O_7(110)$ surface, are not observed for the $Li_2B_4O_7(100)$ surface. This observation of image states for the (110) surface but not the (100) surface is consistent with a greater defect density at the $Li_2B_4O_7(100)$ surface.

In spite of the partial density of states calculated in the local density approximation [10], there is resonant enhancement of the valence band maximum at a photon energy roughly corresponding to the Li1s core threshold of about 55 to 56 eV [12], as seen in Figure 5. This indicates that there is a hybridized lithium contribution at the valence band maximum. This particular feature can be reasonably explained as an Auger electron or Coster-Kronig process of a Li1s electron photoexcitation to unoccupied 2p conduction band state, followed by resonant photoemission leaving the same final state as direct photoemission from the states at the valence band maximum. Such a lithium contribution, indicated by the resonant enhancement of the valence band maximum in photoemission at the lithium 1s core edge, along with boron weight added to the valence band maximum, could contribute to a more polar (100) surface in the presence of surface oxygen vacancies. The lithium atoms are localized at the interstices along the longitudinal axis of the crystal lattice [1–6,25,38], so this would not be entirely unexpected.

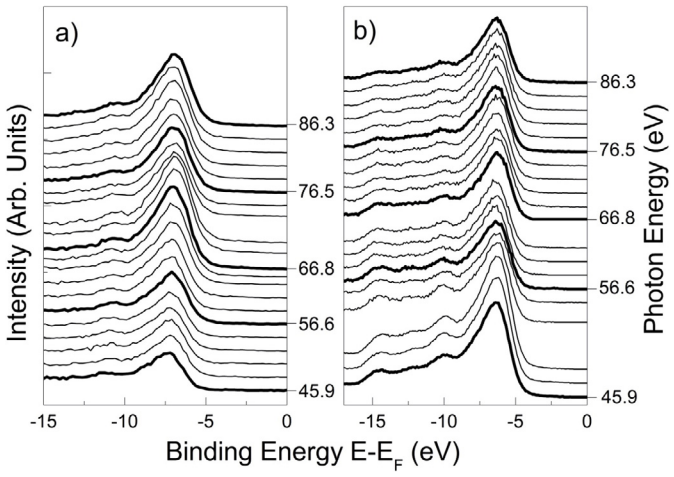

Fig. 6. The photon energy dependent photoemission spectra for both the (a) $Li_2B_4O_7(110)$ and (b) $Li_2B_4O_7(100)$ surfaces. The binding energy of occupied valence band features appears to vary little with changing photon energy. Results for (a) $Li_2B_4O_7(110)$, with the in-plane component of the incident light **E** oriented along [1̲10], and for (b) $Li_2B_4O_7$ (100), with the in-plane component of the incident light **E** oriented along [010]. The light incidence angle was 45 degrees, and the photoelectrons were collected along the surface normal. The occupied state binding energies are given in terms of E-E_F.

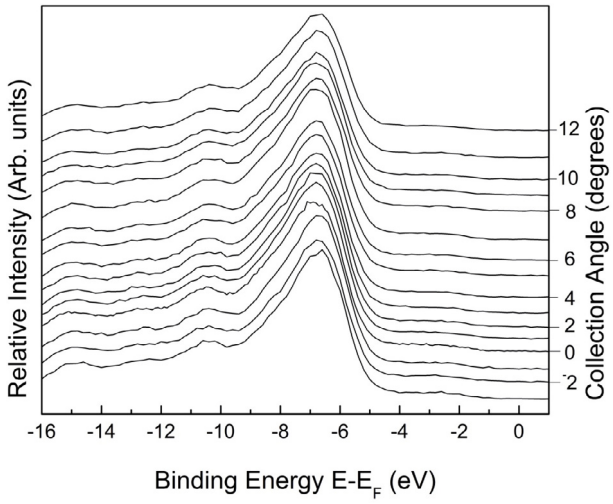

Fig. 7. The emission angle dependent photoemission spectra for the $Li_2B_4O_7(110)$ taken with increasing (emission angle) wave vector along the [1̲10] direction. The light incidence angle was 45 degrees and the spectra were taken at a photon energy of 56 eV. The occupied state binding energies are given in terms of E-E_F.

5 The electronic bulk band structure

The general prediction that the hole mass should be far greater than the electron mass, based on the calculated band structure, is supported by the experimental band mappings of the $Li_2B_4O_7(100)$ and $Li_2B_4O_7(110)$ surfaces. There is no evidence for dispersion, or wave vector dependent changes in binding energy, with either photon energy or emission angle for the filled states, as seen in Figure 6 and Figure 7, respectively. Bulk band structure effects should be evident in the photon energy dependent photoemission spectra. While the perpendicular component of the crystal wave vector ($k_\perp$) is not conserved across the solid vacuum interface, there should be wave vector dependence nonetheless [41–43]:

$$k_\perp = \left(\frac{2m}{\hbar^2}\left\{E_{Kin}(\cos(\theta))^2 + U_0\right\}\right)^{1/2} \quad (1)$$

where U_0 is the inner potential or roughly the occupied band width. No such wave vector dependence is observed in the photon energy dependent photoemission spectra, as illustrated in Figure 6 for both the $Li_2B_4O_7(100)$ and $Li_2B_4O_7(110)$ surfaces.

Similarly, the parallel momentum ($k_{||}$) can be derived as follows from the photoelectron kinetic energy and the emission angle (θ) with respect to the surface normal [41–43]:

$$k_{||} = \sqrt{\frac{2m}{\hbar^2}E_{Kin}}\sin(\theta) = 0.51198\sqrt{E_{Kin}\{\text{eV}\}} \times \sin(\theta)\left\{\text{Å}^{-1}\right\}. \quad (2)$$

Again, both the $Li_2B_4O_7(110)$ and $Li_2B_4O_7(100)$ surfaces exhibit equally little valence band dispersion, with wave vector ($k_{||}$) parallel to either surface along the high symmetry directions of the surface Brillouin zones for each surface. This is illustrated for the $Li_2B_4O_7(110)$ surface, by the emission angle dependent photoemission spectra shown in Figure 7.

Periodic wave vector dependence of shallow core levels have been observed for oxides with large real space unit cells, and thus small Brillouin zones, as in the case of monoclinic Gd_2O_3(–402) [32]. The absence of any such dispersion suggests that the occupied states for both the $Li_2B_4O_7(110)$ and $Li_2B_4O_7(100)$ surfaces are very heavy mass. From the absence of dispersion in the photoemission data (Figs. 6 and 7), we can assign a lower bound to the hole effective mass of about 10 [m^*/m_e]. This lower bound is limited by the feature widths in photoemission, and the limited wave vector and energy resolution.

The absence of dispersion with photon energy is often attributed to conservation of two dimensionality of state, that is to say a surface state. We do not believe that this is the case here as these occupied states, aside from the surface state identified above, do not fall into a gap of the projected band structure and indeed are heavy mass states that simply do not disperse very much. Nor can the problem with the dispersion be related to disorder at the surface: the inverse photoemission exhibits band dispersion consistent with the surface Brillouin zone. Very heavy hole or occupied band state masses for both the $Li_2B_4O_7(110)$ and $Li_2B_4O_7(100)$ crystallographic orientations are consistent with the DFT [10] and LDA [11] band structure calculations.

In contrast to the results garnered from the angle-resolved photoemission, dispersion is evident in empty states observed in the angle-resolved inverse

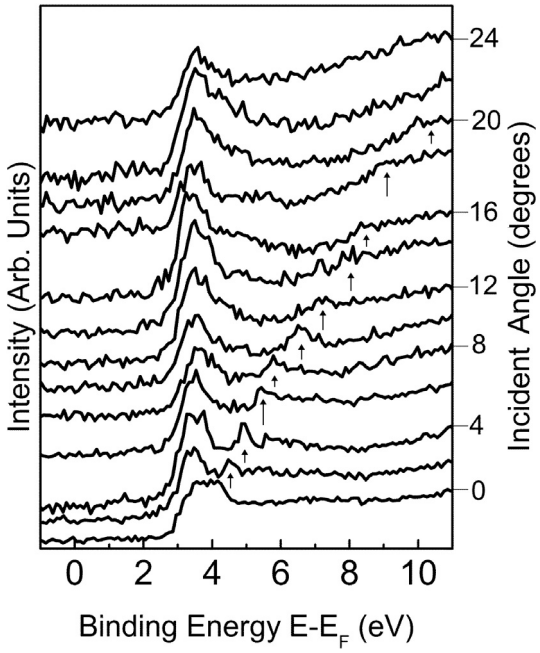

Fig. 8. The incidence angle dependent inverse photoemission spectra for the $Li_2B_4O_7(110)$ with increasing incidence angle (wave vector) along the [$\underline{1}$10] direction. The image state wave vector dependent (incidence angle) dispersion (see text) is indicated by the arrows. The unoccupied state binding energies are given in terms of E-E_F.

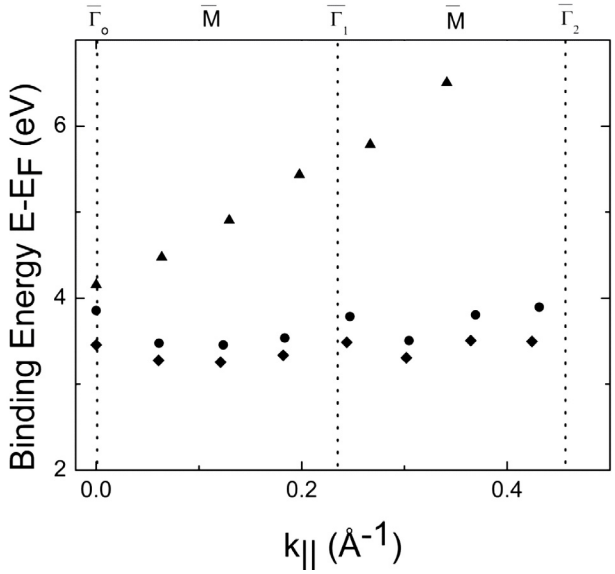

Fig. 9. The unoccupied state binding energies versus the surface parallel wave vector are mapped for the $Li_2B_4O_7(110)$ along the [$\underline{1}$10] direction. The surface Brillouin zone critical points are denoted at top.

photoemission results, obtained as a function of electron incidence angle (θ), as seen in Figure 8. Using the incident electron kinetic energy and equation (2) [33,44], an experimental unoccupied state band dispersion has been mapped, as shown in Figure 9. Despite of the much lower resolution of inverse photoemission, one is able to observe

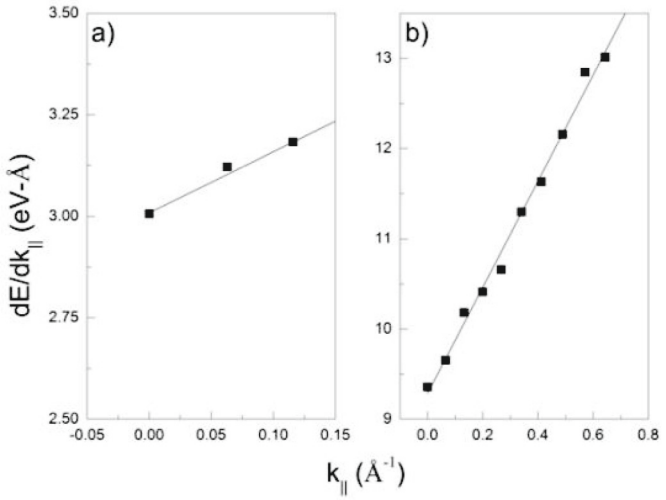

Fig. 10. $dE/dk_{||}$ versus $k_{||}$ of unoccupied states for (a) $Li_2B_4O_7(100)$ LUMO oriented along [011] and the $Li_2B_4O_7(110)$ image state oriented along [$\underline{1}$10], in the reduced Brillouin zone scheme, extracted from inverse photoemission.

dispersion of the bands at the conduction band minimum, as shown in Figures 8 and 9. The periodicity of the dispersion, of the states at the conduction band minimum, is consistent with the expected Brillouin zone of the $Li_2B_4O_7(110)$ surface, as plotted in Figure 9, along both the [001] and [$\underline{1}$10] directions. Again, this could be related to the surface electronic structure, particularly as inverse photoemission is notoriously surface sensitive, but these states do not fall into a gap of the projected bulk band structure.

The trend of the dispersion of the states at the conduction band minimum, towards the Fermi level with increasing wave vector away from the center of the surface Brillouin zone, is qualitatively the opposite of the DFT calculation [10]. Although the LDA calculation of Adamiv and coworkers [11] provides a much smaller band gap than observed in the combined photoemission and inverse photoemission, the trend of the dispersion towards the Fermi level with increasing wave vector away from the center of the surface Brillouin zone seen is consistent with experiment. We can make an estimate of the electron effective masses for the unoccupied $Li_2B_4O_7(110)$ states near the conduction band minimum to be in the region of -0.15 ± 0.1 $[m^*/m_e]$, as indicated in Figure 10. For $Li_2B_4O_7(100)$ states near the conduction band minimum, the effective mass is also in the region of -0.15 ± 0.1 $[m^*/m_e]$.

A nearly parabolic lighter mass band is also seen to disperse independent of the surface Brillouin zone, as shown in Figures 8 and 9, again along both the along [001] and [$\underline{1}$10] directions. This latter very lighter mass band observed for the $Li_2B_4O_7(110)$ surface, along both the along [001] and [$\underline{1}$10] directions of the surface Brillouin zone, at binding energies (E-E_F) well above the Fermi level is an image state, as discussed below. In fact, there was no image potential state observed for the $Li_2B_4O_7(100)$ surface.

6 The image state at the $Li_2B_4O_7(110)$ surface

Image states are characteristic of clean, flat, largely defect free surfaces. The absence of any image states for the $Li_2B_4O_7(100)$ surface is consistent with the presence of defects at this surface; defects which are very likely surface oxygen vacancies, as has been noted above. The presence of an image state for the $Li_2B_4O_7(110)$ surface (Figs. 8 and 9), indicates that this surface is largely defect free with a very flat surface potential. We note that the $Li_2B_4O_7(110)$ surface image state dispersion is not periodic in nature and, in fact, is seen to be simply parabolic both the [001] and [$\underline{1}$10] directions of the surface Brillouin zone. The surface potential of the $Li_2B_4O_7(110)$ surface must be so flat that the image state is not perturbed by the surface crystallography, and disperses almost independently of the surface Brillouin zone (Figs. 8 and 9).

While, as we noted above, the $Li_2B_4O_7(110)$ surface is distinguished by a surface state within a gap of the projected bulk band structure (Figs. 3 and 4), this surface also exhibits very little light polarization dependence of the bulk valence band states (Fig. 3). As has been determined previously, this same surface is also characterized by an off-axis pyroelectric effect [9]. Both effects may combine to reduce the surface potential variations leading to a parabolic image potential state. What is also evident is that the image state for the $Li_2B_4O_7(110)$ surface possesses a very light effective mass of $m^*/m_e = 0.06 \pm 0.02$. Such a light mass state might well reside well above the surface potential and show little scattering with the surface lattice.

7 Summary

We find from combined photoemission and inverse photoemission studies that the bulk band gap for both the $Li_2B_4O_7(110)$ and $Li_2B_4O_7(100)$ surfaces is in the vicinity of 8.9 to 10.1 eV, but generally between 9.8 and 10.1 eV. These values are qualitatively similar to DFT/LDA ground state models [10]. Both the $Li_2B_4O_7(110)$ and $Li_2B_4O_7(100)$ surfaces are n-type, consistent with oxygen vacancies, although (100) is more n-type than (110), possibly due to a higher concentration of oxygen vacancies at the (100) surface. Consistent with recent band structure calculations [10,11], the occupied states show much less dispersion than the unoccupied states with an effective mass in the region of -0.15 ± 0.1 $[m^*/m_e]$. The dispersion of the states near the conduction band minimum shows qualitative agreement with one band structure calculation for this material [11] but not the other [10]. From our results, clear, periodic dispersion is observed in the unoccupied states.

In addition, there is an image state for the $Li_2B_4O_7(110)$ surface with a very light effective mass of $m^*/m_e = 0.06 \pm 0.02$. This is a very surprising result suggesting that well ordered compositionally uniform surfaces of $Li_2B_4O_7(110)$ are possible.

This work was supported by the Defense Threat Reduction Agency (Grant No. HDTRA1-07-1-0008 and BRBAA08-I-2-0128), and the Nebraska Research Initiative. We thank M.W. Swinney, Shan Yang, A.T. Brant, and L.E. Halliburton for the EPR and ENDOR measurements and acknowledge some helpful discussions with Alastair McLean. This work was undertaken in partial fulfillment of the doctoral degree at AFIT by one author (DW). The views expressed in this article are those of the authors and do not reflect the official policy or position of the Air Force, Department of Defense or the US Government.

References

1. J. Krogh-Moe, Acta Crystallogr. **15**, 190 (1962)
2. J. Krogh-Moe, Acta Crystallogr. **24**, 179 (1968)
3. M. Natarajan, R. Faggiani, I.O. Brown, Cryst. Struct. Commun. **8**, 367 (1979)
4. S.V. Radaev, L.A. Muradyan, L.F. Malakhova, Y.V. Burak, V.I. Simonov, Kristallografiya **34**, 1400 (1989)
5. Y.V. Burak, B.V. Padlyak, V.M. Shevel, Radiat. Effects Defects Solids **157**, 1101 (2002)
6. V.T. Adamiv, Y.V. Burak, I.M. Teslyuk, J. Cryst. Growth **289**, 157 (2006)
7. Y.V. Burak, J. Phys. Stud. **2**, 62 (1998)
8. A.S. Bhalla, L.E. Cross, R.H. Whatmore, Jpn J. Appl. Phys. Suppl. **24**, 727 (1985)
9. I. Ketsman, D. Wooten, J. Xiao, Y.B. Losovyj, Y.V. Burak, V.T. Adamiv, A. Sokolov, J. Petrosky, J. McClory, P.A. Dowben, Phys. Lett. A **374**, 891 (2010)
10. M.M. Islam, V.V. Maslyuk, T. Bredow, C. Minot, J. Phys. Chem. B **109**, 13597 (2005)
11. V.T. Adamiv, Y.V. Burak, I.V. Kityk, J. Kasperczyk, R. Smok, M. Czerwinski, Opt. Mater. **8**, 207 (1997); Y.V. Burak, Y.O. Dovgyi, I.V. Kityk, Sol. State Phys. **31**, 275 (1989)
12. D. Wooten, I. Ketsman, Jie Xiao, Y.B. Losovyj, J. Petrosky, J. McClory, Y.V. Burak, V.T. Adamiv, P.A. Dowben, Physica B **405** 461 (2010)
13. D. Wooten, I. Ketsman, J. Xiao, Y.B. Losovyj, J. Petrosky, J. McClory, Y.V. Burak, V.T. Adamiv, P.A. Dowben, Mater. Res. Soc. Symp. Proc. **1164**, L04-04 (2009)
14. Sangeeta, K. Chennakesavulu, D.G. Deai, S.C. Sabharwal, M. Alex, M.D. Ghodgaonkar, Nucl. Instrum. Meth. Phys. Res. A **571**, 699 (2007)
15. Y.V. Burak, V.T. Adamiv, I.M. Teslyuk, V.M. Shevel, Radiat. Meas. **38**, 681 (2004)
16. H. Werheit, J. Phys.: Condens. Matter **18**, 10655 (2006)
17. H. Werheit, J. Phys.: Condens. Matter **19**, 186207 (2007)
18. A.N. Caruso, R.B. Billa, S. Balaz, Jennifer I. Brand, P.A. Dowben, J. Phys.: Condens. Matter **16**, L139 (2004)
19. B.W. Robertson, S. Adenwalla, A. Harken, P. Welsch, J.I. Brand, P.A. Dowben, J.P. Claassen, Appl. Phys. Lett. **80**, 3644 (2002)
20. B.W. Robertson, S. Adenwalla, A. Harken, P. Welsch, J.I. Brand, J.P. Claassen, N.M. Boag, P.A. Dowben, Proc. SPIE **4785**, 226 (2002)

21. S. Adenwalla, R. Billa, J.I. Brand, E. Day, M.J. Diaz, A. Harken, A.S. McMullenGunn, R. Padmanabhan, B.W. Robertson, Proc. SPIE **5199**, 70 (2003)
22. K. Osberg, N. Schemm, S. Balkir, J.I. Brand, S. Hallbeck, P. Dowben, M.W. Hoffman, IEEE Sens. J. **6**, 1531 (2006)
23. K. Osberg, N. Schemm, S. Balkir, J.I. Brand, S. Hallbeck, P. Dowben, *Proc. IEEE Int. Symp. on Circuits and Systems (ISCAS)* (2006), p. 1179
24. A.N. Caruso, P.A. Dowben, S. Balkir, N. Schemm, K. Osberg, R.W. Fairchild, O.B. Flores, S. Balaz, A.D. Harken, B.W. Robertson, J.I. Brand, Mater. Sci. Eng. B **135**, 129 (2006)
25. E. Day, M.J. Diaz, S. Adenwalla, J. Phys. D: Appl. Phys. **39**, 2920 (2006)
26. V.M. Holovey, V.I. Sidey, V.I. Lyamayev, P.P. Puga, J. Lumin. **126**, 408 (2007)
27. D. Podgórska, S.M. Kaczmarek, W. Drozdowski, M. Berkowski, A. Worsztynowicz, Acta Phys. Polon. A **107**, 507 (2005)
28. G.I. Malovichko, V.G. Grachev, A.O. Matkovskii, Sov. Phys. Solid State **33**, 1107 (1991)
29. Y. Losovyj, I. Ketsman, E. Morikawa, Z. Wang, J. Tang, P. Dowben, Nucl. Instrum. Meth. A **582**, 264 (2007)
30. P.A. Dowben, D. LaGraffe, M. Onellion, J. Phys.: Condens. Matter **1**, 6571 (1989)
31. J. Hormes, J.D. Scott, V.P. Suller, Synchrotron Radiat. News **19**, 27 (2006)
32. Y.B. Losovyj, D. Wooten, J. Colon Santana, J.M. An, K.D. Belashchenko, N. Lozova, J. Petrosky, A. Sokolov, J. Tang, W. Wang, N. Arulsamy, P.A. Dowben, J. Phys.: Condens. Matter **21**, 045602 (2009)
33. D.-Q. Feng, D. Wisbey, Y.B. Losovyj, Y. Tai, M. Zharnikov, P.A. Dowben, Phys. Rev. B **74**, 165425 (2006)
34. J. Xiao, L.G. Rosa, M. Poulsen, D.-Q. Feng, S. Reddy, J.M. Takacs, L. Cai, J. Zhang, S. Ducharme, P.A. Dowben, J. Phys. Condens. Matter **18**, L155 (2006)
35. J. Choi, P.A. Dowben, S. Ducharme, V.M. Fridkin, S.P. Palto, N. Petukhova, S.G. Yudin, Phys. Lett. A **249**, 505 (1998)
36. C.N. Borca, T. Komesu, P.A. Dowben, J. Electron. Spectrosc. Relat. Phenom. **122**, 259 (2002)
37. D.N. McIlroy, J. Zhang, P.A. Dowben, D. Heskett, Mater. Sci. Eng. A **217-218**, 439 (1996)
38. A.Y. Kuznetsov, A.V. Kruzhalov, I.N. Ogorodnikov, A.B. Sobolev, L.I. Isaenko, Phys. Solid State **41**, 48 (1999)
39. C. Sebenne, Il Nuovo Cimento B (1971-1996) **39**, 768 (1977)
40. R. Manzke, M. Skibowski, Phys. Scr. **T31**, 87 (1990)
41. E.W. Plummer, W. Eberhardt, Adv. Chem. Phys. **49**, 533 (1982)
42. N.V. Richardson, A.M. Bradshaw, in *Electron Spectroscopy: Theory, Techniques and Applications*, Vol. 4, edited by C.R. Brundle, A.D. Baker (Academic Press, San Diego 1984), p. 153
43. P.A. Dowben, J. Choi, E. Morikawa, B. Xu, The Band Structure and Orientation of Molecular Adsorbates on Surfaces by Angle-Resolved Electron Spectroscopies, in *Handbook of Thin Films, Characterization and Spectroscopy of Thin Films*, Vol. 2, edited by H.S. Nalwa (Academic Press, 2002), Chap. 2, pp. 61–114
44. N.V. Smith, Rep. Prog. Phys. **51**, 1227 (1988)